rPOP: Robust PET-Only Processing of community acquired heterogeneous amyloid-PET data

Leonardo Iaccarino[a], Renaud La Joie[a], Robert Koeppe[b], Barry A. Siegel[c], Bruce E. Hillner[d], Constantine Gatsonis[e,f], Rachel A. Whitmer[g,h], Maria C. Carrillo[i], Charles Apgar[j], Monica R. Camacho[k,l], Rachel Nosheny[k,m], Gil D. Rabinovici[a,n] , Alzheimer's Disease Neuroimaging Initiative*

[a] Memory and Aging Center, Department of Neurology, Weill Institute for Neurosciences, University of California San Francisco, San Francisco, CA, USA
[b] Department of Radiology, University of Michigan, Ann Arbor, MI, USA.
[c] Edward Mallinckrodt Institute of Radiology, Washington University School of Medicine in St Louis, St Louis, MO, USA
[d] Department of Medicine, Virginia Commonwealth University, Richmond, VA, USA
[e] Center for Statistical Sciences, Brown University School of Public Health, Providence, RI, USA
[f] Department of Biostatistics, Brown University School of Public Health, Providence, RI, USA
[g] Division of Research, Kaiser Permanente, Oakland, CA, USA
[h] Department of Public Health Sciences, University of California Davis, Davis, CA, USA
[i] Medical and Scientific Relations Division, Alzheimer's Association, Chicago, IL, USA
[j] American College of Radiology, Reston, VA, USA
[k] San Francisco VA Medical Center, San Francisco, CA, USA
[l] Northern California Institute for Research and Education (NCIRE), San Francisco, CA, USA
[m] Department of Psychiatry, University of California San Francisco, San Francisco, CA, USA
[n] Department of Radiology and Biomedical Imaging, University of California San Francisco, San Francisco, CA, USA

* Data used in preparation of this article were obtained from the Alzheimer's Disease Neuroimaging Initiative (ADNI) database (adni.loni.usc.edu). As such, the investigators within the ADNI contributed to the design and implementation of ADNI and/or provided data but did not participate in analysis or writing of this report. A complete listing of ADNI investigators can be found at: http://adni.loni.usc.edu/wp-content/uploads/how_to_apply/ADNI_Acknowledgement_List.pdf

Table of Content

1. Centiloid Scale Calibration

Level 1. We first replicated Level-1 analysis following instructions in (Klunk et al., 2015), however using SPM12 and not SPM8 for the image processing. We downloaded the 79 PiB-PET 50-70 min scans from GAAIN, estimating neocortical SUVRs using the whole cerebellum reference region. The individual absolute differences with GAAIN data ranged between 0.01%<x<3.93%, meeting the requirement (<5%). We observed a mean PIBwc SUVR for the AD participants of 2.078 (original 2.076) and for the YC of 1.011 (original 1.009).

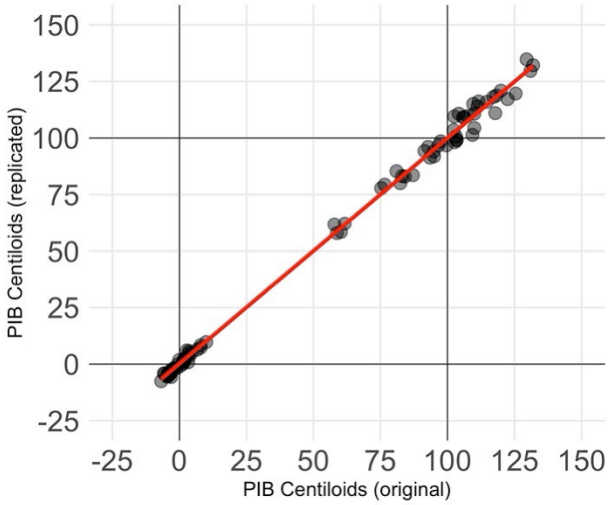

Centiloid Figure 1. Linear fit for observed and published GAAIN Centiloids

Based on this, our PIB Centiloid conversion formula was:

$$PIBCL = 100 * (PIBSUVRind - 1.011)/1.067$$

We then estimated Centiloids, yielding a linear fit with the published Centiloid values meeting all the requirements (Klunk et al., 2015), i.e., an R^2 of 0.997 (required >.98), a slope of 0.998 (required between 0.98<x<1.02) and an intercept of 0.11 (required between -2<x<2) (see also Figure 1).

Level 2. To calibrate the Centiloid conversion formula, we proceeded to download and process the GAAIN datasets for ^{18}F-florbetapir (FBP), ^{18}F-florbetaben (FBB) and ^{18}F-flutemetamol (FLUTE).

^{18}F-Florbetapir-PET. The FBP-PET dataset consists of 46 subjects, 33 older and 13 young controls, with 50-60min FBP-PET and 50-70 PiB-PET scans (Navitsky et al., 2018). We processed the PiB-PET scans with the standard Centiloid approach, processing the FBP-PET scans with rPOP. PIB-PET standard and FBP-PET rPOP-based SUVRs were highly correlated (R^2:0.883, required >0.7). Based on slope and intercept, we first converted rPOP FBP-PET SUVRs in standard PIB-PET SUVRs (Eq 2.2.3.2b), then applied the Centiloid conversion formula (Eq 2.2.3).

$$Eq.\ 2.2.3.2b: PIBCalcSUVRIND = \frac{(FBPSUVRind\ - 0.61290)}{0.49361}$$

$$Eq. 2.2.3: PIBCalcCL = 100 * \frac{(PIBCalcSUVRIND - 1.011)}{1.067}$$

Based on the converted Centiloids, the final formula to directly convert FBP-PET rPOP neocortical SUVRs to Centiloids was (see also Figure 2):

$$FBPCL = (189.9 * FBPSUVRind) - 211.1$$

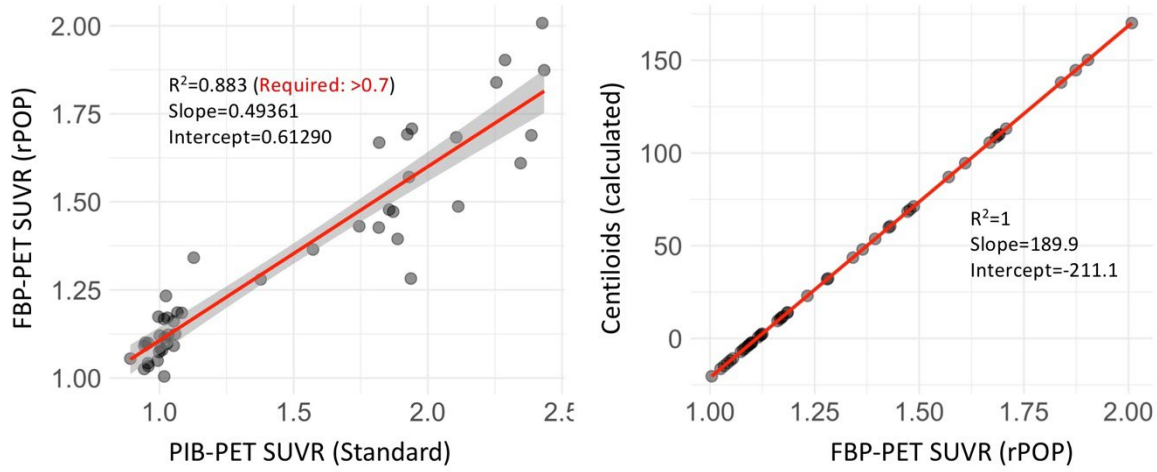

Centiloid Figure 2. Level 2 FBP-PET processing

^{18}F-Florbetaben-PET. The FBB-PET dataset consists of 35 subjects, 25 older and 10 young controls, with 90-110min FBB-PET and 50-70 PiB-PET scans (Rowe et al., 2017). We processed the PiB-PET scans with the standard Centiloid approach, processing the FBB-PET scans with rPOP. PIB-PET standard and FBB-PET rPOP-based SUVRs were highly correlated (R^2:0.9613, required >0.7). Based on slope and intercept, we first converted rPOP FBB-PET SUVRs into standard PIB-PET SUVRs (Eq 2.2.3.2b), then applied the Centiloid conversion formula (Eq 2.2.3).

$$Eq.\ 2.2.3.2b: PIBCalcSUVRIND = \frac{(FBBSUVRind\ - 0.46349)}{0.58321}$$

$$Eq.\ 2.2.3: PIBCalcCL = 100 * \frac{(PIBCalcSUVRIND - 1.011)}{1.067}$$

Based on the converted Centiloids, the final formula to directly convert FBB-PET rPOP neocortical SUVRs to Centiloids was (see also Figure 3):

$$FBBCL = (160.7 * FBBSUVRind) - 169.2$$

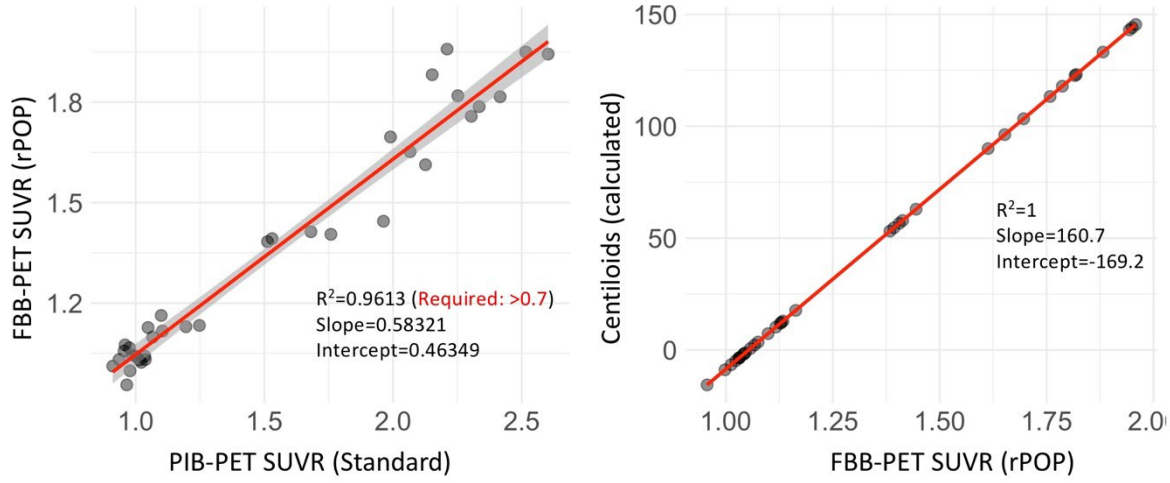

Centiloid Figure 3. Level 2 FBB-PET processing

^{18}F-Flutemetamol-PET. The FLUTE-PET dataset consists of 74 subjects, 50 subjects with likely high amyloid burden (Alzheimer's Disease (AD), aMCI and older (45+yrs) healthy controls) and 24 young healthy volunteers, with 90-110min FLUTE-PET and 50-70 PiB-PET scans (Battle et al., 2018). We processed the PiB-PET scans with the standard Centiloid approach, processing the FLUTE-PET scans with rPOP. PIB-PET standard and FLUTE-PET rPOP-based SUVRs were highly correlated (R^2:0.9529, required >0.7). Based on slope and intercept, we first converted rPOP FLUTE-PET SUVRs into standard PIB-PET SUVRs (Eq 2.2.3.2b), then applied the Centiloid conversion formula (Eq 2.2.3).

$$Eq.\,2.2.3.2b: PIBCalcSUVRIND = \frac{(FLUTESUVRind\ - 0.32489)}{0.73463}$$

$$Eq.\,2.2.3: PIBCalcCL = 100 * \frac{(PIBCalcSUVRIND - 1.011)}{1.067}$$

Based on the converted Centiloids, the final formula to directly convert FLUTE-PET rPOP neocortical SUVRs to Centiloids was (see also Figure 4):

$$FLUTECL = (127.6 * FLUTESUVRind) - 136.2$$

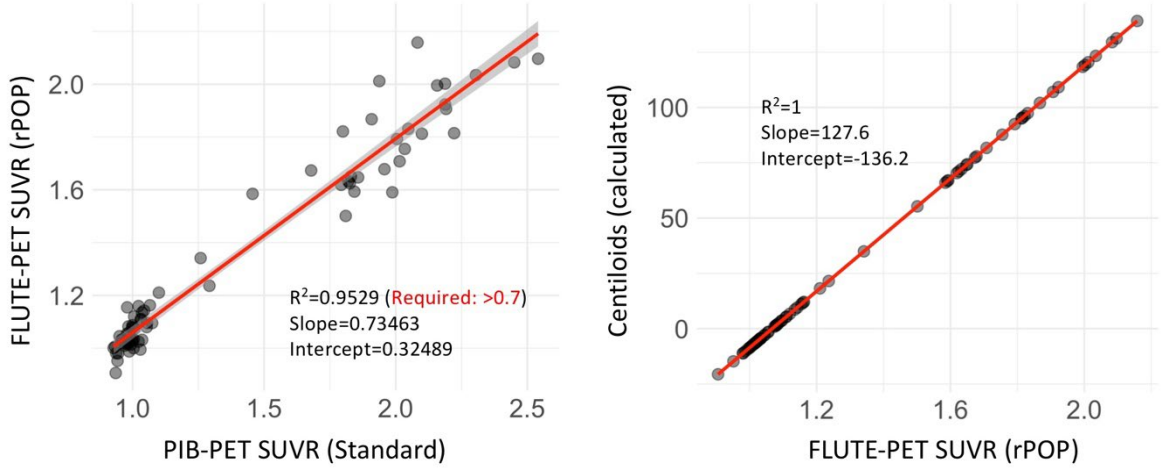

Centiloid Figure 4. Level 2 FLUTE-PET processing

Supplementary Table 1. Demographic and clinical summary

Cohort	IDEAS-BHR	ADNI
N	663	1,518
Age mean(sd)	73.9(5.7)	73.2(7.5)
Sex[1] N M/F	360/292	773/745
MMSE[2,3] mean(sd)	26.9(3.2)	27.6(2.9)
Clinical Stage N CN/MCI/Dementia	0/527/136	622/653/243
Amyloid-PET Radiotracer N FBP/FBB/FLUTE	465/165/33	1249/269/0

Legend: N=Number, sd=standard deviation, MMSE=MiniMental Status Examination, CN=Cognitively Normal, MCI=Mild Cognitive Impairment, FBP= ^{18}F-florbetapir, FBB=^{18}F-florbetaben, FLUTE=^{18}F-flutemetamol

[1] N=11 missing for IDEAS-BHR dataset
[2] MMSE for IDEAS-BHR dataset also included converted Montreal Cognitive Assessment (MoCA) scores for a subset of participants (N=187/663) (Roalf et al., 2013)
[3] MMSE at PET-time was missing for N=63 ADNI participants

Supplementary Table 2. Summary of FWHM estimations from 3dFWHMx

Cohort	IDEAS-BHR	ADNI	Cohen's d	p
N	663	1,518		
FWHM x mean(sd)	9.1(2.16)	5.85(1.98)	1.59	<0.001
FWHM y mean(sd)	8.28(1.98)	5.32(1.78)	1.6	<0.001
FWHM z mean(sd)	8.51(1.57)	5.84(1.7)	1.6	<0.001
FWHM avg mean(sd)	8.63(1.73)	5.67(1.77)	1.68	<0.001

Legend: N=Number, FWHM=Full-Width at Half Maximum, sd=standard deviation

Supplementary Table 3. Cross-validation of regional FBP SUVR quantification in MRI-based vs. rPOP-based warped PET SUVR images

Tracer	roi_id	Label	r	Pval_FDR
FBP	169	Left PCu precuneus	0.99	<0.001
FBP	140	Right MFC medial frontal cortex	0.99	<0.001
FBP	168	Right PCu precuneus	0.99	<0.001
FBP	141	Left MFC medial frontal cortex	0.99	<0.001
FBP	152	Right MSFG superior frontal gyrus medial segment	0.98	<0.001
FBP	153	Left MSFG superior frontal gyrus medial segment	0.98	<0.001
FBP	193	Left SMC supplementary motor cortex	0.98	<0.001
FBP	101	Left ACgG anterior cingulate gyrus	0.98	<0.001
FBP	100	Right ACgG anterior cingulate gyrus	0.98	<0.001
FBP	166	Right PCgG posterior cingulate gyrus	0.98	<0.001
FBP	138	Right MCgG middle cingulate gyrus	0.98	<0.001
FBP	167	Left PCgG posterior cingulate gyrus	0.98	<0.001
FBP	207	Left TTG transverse temporal gyrus	0.98	<0.001
FBP	206	Right TTG transverse temporal gyrus	0.98	<0.001
FBP	155	Left MTG middle temporal gyrus	0.98	<0.001
FBP	30	Left Accumbens Area	0.97	<0.001
FBP	151	Left MPrG precentral gyrus medial segment	0.97	<0.001
FBP	102	Right AIns anterior insula	0.97	<0.001
FBP	23	Right Accumbens Area	0.97	<0.001
FBP	154	Right MTG middle temporal gyrus	0.97	<0.001
FBP	58	Left Putamen	0.97	<0.001
FBP	57	Right Putamen	0.97	<0.001
FBP	163	Left OpIFG opercular part of the inferior frontal gyrus	0.97	<0.001
FBP	106	Right AnG angular gyrus	0.97	<0.001
FBP	185	Left PT planum temporale	0.97	<0.001
FBP	192	Right SMC supplementary motor cortex	0.97	<0.001
FBP	108	Right Calc calcarine cortex	0.97	<0.001
FBP	150	Right MPrG precentral gyrus medial segment	0.97	<0.001
FBP	201	Left STG superior temporal gyrus	0.97	<0.001
FBP	45	Left Cerebral White Matter	0.97	<0.001
FBP	139	Left MCgG middle cingulate gyrus	0.97	<0.001
FBP	109	Left Calc calcarine cortex	0.97	<0.001
FBP	44	Right Cerebral White Matter	0.97	<0.001
FBP	125	Left GRe gyrus rectus	0.97	<0.001
FBP	187	Left SCA subcallosal area	0.97	<0.001
FBP	103	Left AIns anterior insula	0.97	<0.001
FBP	194	Right SMG supramarginal gyrus	0.97	<0.001
FBP	124	Right GRe gyrus rectus	0.96	<0.001
FBP	165	Left OrIFG orbital part of the inferior frontal gyrus	0.96	<0.001
FBP	107	Left AnG angular gyrus	0.96	<0.001
FBP	202	Right TMP temporal pole	0.96	<0.001
FBP	186	Right SCA subcallosal area	0.96	<0.001

FBP	198	Right SPL superior parietal lobule	0.96	<0.001
FBP	195	Left SMG supramarginal gyrus	0.96	<0.001
FBP	200	Right STG superior temporal gyrus	0.96	<0.001
FBP	203	Left TMP temporal pole	0.96	<0.001
FBP	199	Left SPL superior parietal lobule	0.96	<0.001
FBP	143	Left MFG middle frontal gyrus	0.96	<0.001
FBP	184	Right PT planum temporale	0.96	<0.001
FBP	41	Left Cerebellum White Matter	0.96	<0.001
FBP	172	Right PIns posterior insula	0.96	<0.001
FBP	142	Right MFG middle frontal gyrus	0.95	<0.001
FBP	118	Right FO frontal operculum	0.95	<0.001
FBP	176	Right PoG postcentral gyrus	0.95	<0.001
FBP	162	Right OpIFG opercular part of the inferior frontal gyrus	0.95	<0.001
FBP	175	Left PO parietal operculum	0.95	<0.001
FBP	179	Left POrG posterior orbital gyrus	0.95	<0.001
FBP	174	Right PO parietal operculum	0.95	<0.001
FBP	119	Left FO frontal operculum	0.95	<0.001
FBP	35	Brain Stem	0.95	<0.001
FBP	164	Right OrIFG orbital part of the inferior frontal gyrus	0.95	<0.001
FBP	112	Right CO central operculum	0.95	<0.001
FBP	113	Left CO central operculum	0.95	<0.001
FBP	115	Left Cun cuneus	0.95	<0.001
FBP	177	Left PoG postcentral gyrus	0.95	<0.001
FBP	178	Right POrG posterior orbital gyrus	0.95	<0.001
FBP	40	Right Cerebellum White Matter	0.95	<0.001
FBP	36	Right Caudate	0.95	<0.001
FBP	181	Left PP planum polare	0.95	<0.001
FBP	205	Left TrIFG triangular part of the inferior frontal gyrus	0.95	<0.001
FBP	173	Left PIns posterior insula	0.94	<0.001
FBP	114	Right Cun cuneus	0.94	<0.001
FBP	147	Left MOrG medial orbital gyrus	0.94	<0.001
FBP	190	Right SFG superior frontal gyrus	0.94	<0.001
FBP	148	Right MPoG postcentral gyrus medial segment	0.94	<0.001
FBP	123	Left FuG fusiform gyrus	0.94	<0.001
FBP	191	Left SFG superior frontal gyrus	0.94	<0.001
FBP	37	Left Caudate	0.93	<0.001
FBP	180	Right PP planum polare	0.93	<0.001
FBP	182	Right PrG precentral gyrus	0.93	<0.001
FBP	59	Right Thalamus Proper	0.93	<0.001
FBP	144	Right MOG middle occipital gyrus	0.93	<0.001
FBP	149	Left MPoG postcentral gyrus medial segment	0.93	<0.001
FBP	146	Right MOrG medial orbital gyrus	0.93	<0.001
FBP	48	Left Hippocampus	0.93	<0.001
FBP	104	Right AOrG anterior orbital gyrus	0.93	<0.001
FBP	204	Right TrIFG triangular part of the inferior frontal gyrus	0.93	<0.001
FBP	136	Right LOrG lateral orbital gyrus	0.92	<0.001

FBP	137	Left LOrG lateral orbital gyrus	0.92	<0.001
FBP	61	Right Ventral DC	0.92	<0.001
FBP	132	Right ITG inferior temporal gyrus	0.92	<0.001
FBP	105	Left AOrG anterior orbital gyrus	0.92	<0.001
FBP	183	Left PrG precentral gyrus	0.92	<0.001
FBP	31	Right Amygdala	0.92	<0.001
FBP	133	Left ITG inferior temporal gyrus	0.92	<0.001
FBP	170	Right PHG parahippocampal gyrus	0.92	<0.001
FBP	60	Left Thalamus Proper	0.92	<0.001
FBP	145	Left MOG middle occipital gyrus	0.92	<0.001
FBP	62	Left Ventral DC	0.92	<0.001
FBP	32	Left Amygdala	0.91	<0.001
FBP	135	Left LiG lingual gyrus	0.91	<0.001
FBP	122	Right FuG fusiform gyrus	0.91	<0.001
FBP	128	Right IOG inferior occipital gyrus	0.91	<0.001
FBP	47	Right Hippocampus	0.90	<0.001
FBP	171	Left PHG parahippocampal gyrus	0.90	<0.001
FBP	134	Right LiG lingual gyrus	0.89	<0.001
FBP	120	Right FRP frontal pole	0.89	<0.001
FBP	121	Left FRP frontal pole	0.88	<0.001
FBP	55	Right Pallidum	0.88	<0.001
FBP	116	Right Ent entorhinal area	0.88	<0.001
FBP	129	Left IOG inferior occipital gyrus	0.88	<0.001
FBP	56	Left Pallidum	0.88	<0.001
FBP	117	Left Ent entorhinal area	0.87	<0.001
FBP	38	Right Cerebellum Exterior	0.87	<0.001
FBP	196	Right SOG superior occipital gyrus	0.87	<0.001
FBP	197	Left SOG superior occipital gyrus	0.84	<0.001
FBP	76	Right Basal Forebrain	0.84	<0.001
FBP	75	Left Basal Forebrain	0.83	<0.001
FBP	161	Left OFuG occipital fusiform gyrus	0.82	<0.001
FBP	39	Left Cerebellum Exterior	0.82	<0.001
FBP	160	Right OFuG occipital fusiform gyrus	0.81	<0.001
FBP	73	Cerebellar Vermal Lobules VIII-X	0.80	<0.001
FBP	71	Cerebellar Vermal Lobules I-V	0.80	<0.001
FBP	156	Right OCP occipital pole	0.72	<0.001
FBP	157	Left OCP occipital pole	0.69	<0.001
FBP	72	Cerebellar Vermal Lobules VI-VII	0.69	<0.001

Table showing correlation coefficients estimated based on regional SUVR values extracted from FBP PET images warped to standard space via MRI-based or rPOP-based parameters. The roi_id column refers to the ID of the corresponding region in the atlas provided with the SPM software. ROIs are sorted from highest to lowest correlation coefficients.

Legend: FBP=Florbetapir, r=Pearson Correlation Coefficient, Pval_FDR=respective p-value corrected for False Discovery Rate.

Supplementary Table 4. Cross-validation of regional FBB SUVR quantification in MRI-based vs. rPOP-based warped PET SUVR images

Tracer	roi_id	Label	r	Pval_FDR
FBB	140	Right MFC medial frontal cortex	0.99	<0.001
FBB	141	Left MFC medial frontal cortex	0.99	<0.001
FBB	153	Left MSFG superior frontal gyrus medial segment	0.99	<0.001
FBB	101	Left ACgG anterior cingulate gyrus	0.98	<0.001
FBB	155	Left MTG middle temporal gyrus	0.98	<0.001
FBB	169	Left PCu precuneus	0.98	<0.001
FBB	30	Left Accumbens Area	0.98	<0.001
FBB	152	Right MSFG superior frontal gyrus medial segment	0.98	<0.001
FBB	106	Right AnG angular gyrus	0.98	<0.001
FBB	154	Right MTG middle temporal gyrus	0.98	<0.001
FBB	203	Left TMP temporal pole	0.98	<0.001
FBB	207	Left TTG transverse temporal gyrus	0.98	<0.001
FBB	168	Right PCu precuneus	0.98	<0.001
FBB	193	Left SMC supplementary motor cortex	0.98	<0.001
FBB	100	Right ACgG anterior cingulate gyrus	0.98	<0.001
FBB	202	Right TMP temporal pole	0.97	<0.001
FBB	107	Left AnG angular gyrus	0.97	<0.001
FBB	192	Right SMC supplementary motor cortex	0.97	<0.001
FBB	206	Right TTG transverse temporal gyrus	0.97	<0.001
FBB	23	Right Accumbens Area	0.97	<0.001
FBB	108	Right Calc calcarine cortex	0.97	<0.001
FBB	187	Left SCA subcallosal area	0.97	<0.001
FBB	102	Right AIns anterior insula	0.97	<0.001
FBB	103	Left AIns anterior insula	0.97	<0.001
FBB	185	Left PT planum temporale	0.97	<0.001
FBB	201	Left STG superior temporal gyrus	0.97	<0.001
FBB	198	Right SPL superior parietal lobule	0.97	<0.001
FBB	142	Right MFG middle frontal gyrus	0.97	<0.001
FBB	150	Right MPrG precentral gyrus medial segment	0.96	<0.001
FBB	119	Left FO frontal operculum	0.96	<0.001
FBB	58	Left Putamen	0.96	<0.001
FBB	125	Left GRe gyrus rectus	0.96	<0.001
FBB	162	Right OpIFG opercular part of the inferior frontal gyrus	0.96	<0.001
FBB	186	Right SCA subcallosal area	0.96	<0.001
FBB	199	Left SPL superior parietal lobule	0.96	<0.001
FBB	143	Left MFG middle frontal gyrus	0.96	<0.001
FBB	163	Left OpIFG opercular part of the inferior frontal gyrus	0.96	<0.001
FBB	57	Right Putamen	0.96	<0.001
FBB	144	Right MOG middle occipital gyrus	0.96	<0.001
FBB	179	Left POrG posterior orbital gyrus	0.96	<0.001
FBB	124	Right GRe gyrus rectus	0.96	<0.001
FBB	200	Right STG superior temporal gyrus	0.96	<0.001

FBB	194	Right SMG supramarginal gyrus	0.96	<0.001
FBB	165	Left OrIFG orbital part of the inferior frontal gyrus	0.96	<0.001
FBB	109	Left Calc calcarine cortex	0.96	<0.001
FBB	175	Left PO parietal operculum	0.96	<0.001
FBB	195	Left SMG supramarginal gyrus	0.96	<0.001
FBB	167	Left PCgG posterior cingulate gyrus	0.96	<0.001
FBB	151	Left MPrG precentral gyrus medial segment	0.96	<0.001
FBB	184	Right PT planum temporale	0.96	<0.001
FBB	133	Left ITG inferior temporal gyrus	0.95	<0.001
FBB	123	Left FuG fusiform gyrus	0.95	<0.001
FBB	166	Right PCgG posterior cingulate gyrus	0.95	<0.001
FBB	172	Right PIns posterior insula	0.95	<0.001
FBB	205	Left TrIFG triangular part of the inferior frontal gyrus	0.95	<0.001
FBB	128	Right IOG inferior occipital gyrus	0.95	<0.001
FBB	164	Right OrIFG orbital part of the inferior frontal gyrus	0.95	<0.001
FBB	181	Left PP planum polare	0.95	<0.001
FBB	118	Right FO frontal operculum	0.95	<0.001
FBB	204	Right TrIFG triangular part of the inferior frontal gyrus	0.95	<0.001
FBB	114	Right Cun cuneus	0.94	<0.001
FBB	178	Right POrG posterior orbital gyrus	0.94	<0.001
FBB	122	Right FuG fusiform gyrus	0.94	<0.001
FBB	132	Right ITG inferior temporal gyrus	0.94	<0.001
FBB	190	Right SFG superior frontal gyrus	0.94	<0.001
FBB	105	Left AOrG anterior orbital gyrus	0.94	<0.001
FBB	113	Left CO central operculum	0.94	<0.001
FBB	191	Left SFG superior frontal gyrus	0.94	<0.001
FBB	173	Left PIns posterior insula	0.94	<0.001
FBB	115	Left Cun cuneus	0.94	<0.001
FBB	147	Left MOrG medial orbital gyrus	0.94	<0.001
FBB	146	Right MOrG medial orbital gyrus	0.94	<0.001
FBB	37	Left Caudate	0.94	<0.001
FBB	138	Right MCgG middle cingulate gyrus	0.94	<0.001
FBB	112	Right CO central operculum	0.93	<0.001
FBB	139	Left MCgG middle cingulate gyrus	0.93	<0.001
FBB	104	Right AOrG anterior orbital gyrus	0.93	<0.001
FBB	174	Right PO parietal operculum	0.93	<0.001
FBB	180	Right PP planum polare	0.93	<0.001
FBB	31	Right Amygdala	0.93	<0.001
FBB	32	Left Amygdala	0.93	<0.001
FBB	137	Left LOrG lateral orbital gyrus	0.93	<0.001
FBB	149	Left MPoG postcentral gyrus medial segment	0.93	<0.001
FBB	145	Left MOG middle occipital gyrus	0.93	<0.001
FBB	148	Right MPoG postcentral gyrus medial segment	0.93	<0.001
FBB	120	Right FRP frontal pole	0.93	<0.001
FBB	36	Right Caudate	0.92	<0.001
FBB	171	Left PHG parahippocampal gyrus	0.92	<0.001

FBB	176	Right PoG postcentral gyrus	0.92	<0.001
FBB	45	Left Cerebral White Matter	0.92	<0.001
FBB	44	Right Cerebral White Matter	0.92	<0.001
FBB	121	Left FRP frontal pole	0.92	<0.001
FBB	129	Left IOG inferior occipital gyrus	0.92	<0.001
FBB	182	Right PrG precentral gyrus	0.91	<0.001
FBB	47	Right Hippocampus	0.91	<0.001
FBB	136	Right LOrG lateral orbital gyrus	0.90	<0.001
FBB	170	Right PHG parahippocampal gyrus	0.90	<0.001
FBB	41	Left Cerebellum White Matter	0.90	<0.001
FBB	60	Left Thalamus Proper	0.90	<0.001
FBB	75	Left Basal Forebrain	0.90	<0.001
FBB	116	Right Ent entorhinal area	0.90	<0.001
FBB	196	Right SOG superior occipital gyrus	0.89	<0.001
FBB	117	Left Ent entorhinal area	0.89	<0.001
FBB	48	Left Hippocampus	0.89	<0.001
FBB	135	Left LiG lingual gyrus	0.89	<0.001
FBB	134	Right LiG lingual gyrus	0.89	<0.001
FBB	59	Right Thalamus Proper	0.89	<0.001
FBB	177	Left PoG postcentral gyrus	0.88	<0.001
FBB	76	Right Basal Forebrain	0.88	<0.001
FBB	40	Right Cerebellum White Matter	0.88	<0.001
FBB	183	Left PrG precentral gyrus	0.87	<0.001
FBB	197	Left SOG superior occipital gyrus	0.86	<0.001
FBB	39	Left Cerebellum Exterior	0.84	<0.001
FBB	38	Right Cerebellum Exterior	0.84	<0.001
FBB	35	Brain Stem	0.83	<0.001
FBB	160	Right OFuG occipital fusiform gyrus	0.82	<0.001
FBB	56	Left Pallidum	0.80	<0.001
FBB	55	Right Pallidum	0.79	<0.001
FBB	161	Left OFuG occipital fusiform gyrus	0.79	<0.001
FBB	62	Left Ventral DC	0.79	<0.001
FBB	157	Left OCP occipital pole	0.77	<0.001
FBB	156	Right OCP occipital pole	0.75	<0.001
FBB	61	Right Ventral DC	0.75	<0.001
FBB	72	Cerebellar Vermal Lobules VI-VII	0.74	<0.001
FBB	71	Cerebellar Vermal Lobules I-V	0.72	<0.001
FBB	73	Cerebellar Vermal Lobules VIII-X	0.60	<0.001

Table showing correlation coefficients estimated based on regional SUVR values extracted from FBB PET images warped to standard space via MRI-based or rPOP-based parameters. The roi_id column refers to the ID of the corresponding region in the atlas provided with the SPM software. ROIs are sorted from highest to lowest correlation coefficients.

Legend: FBB=Florbetaben, r=Pearson Correlation Coefficient, Pval_FDR=respective p-value corrected for False Discovery Rate.

Supplementary Figure 1. Templates for non-linear warping

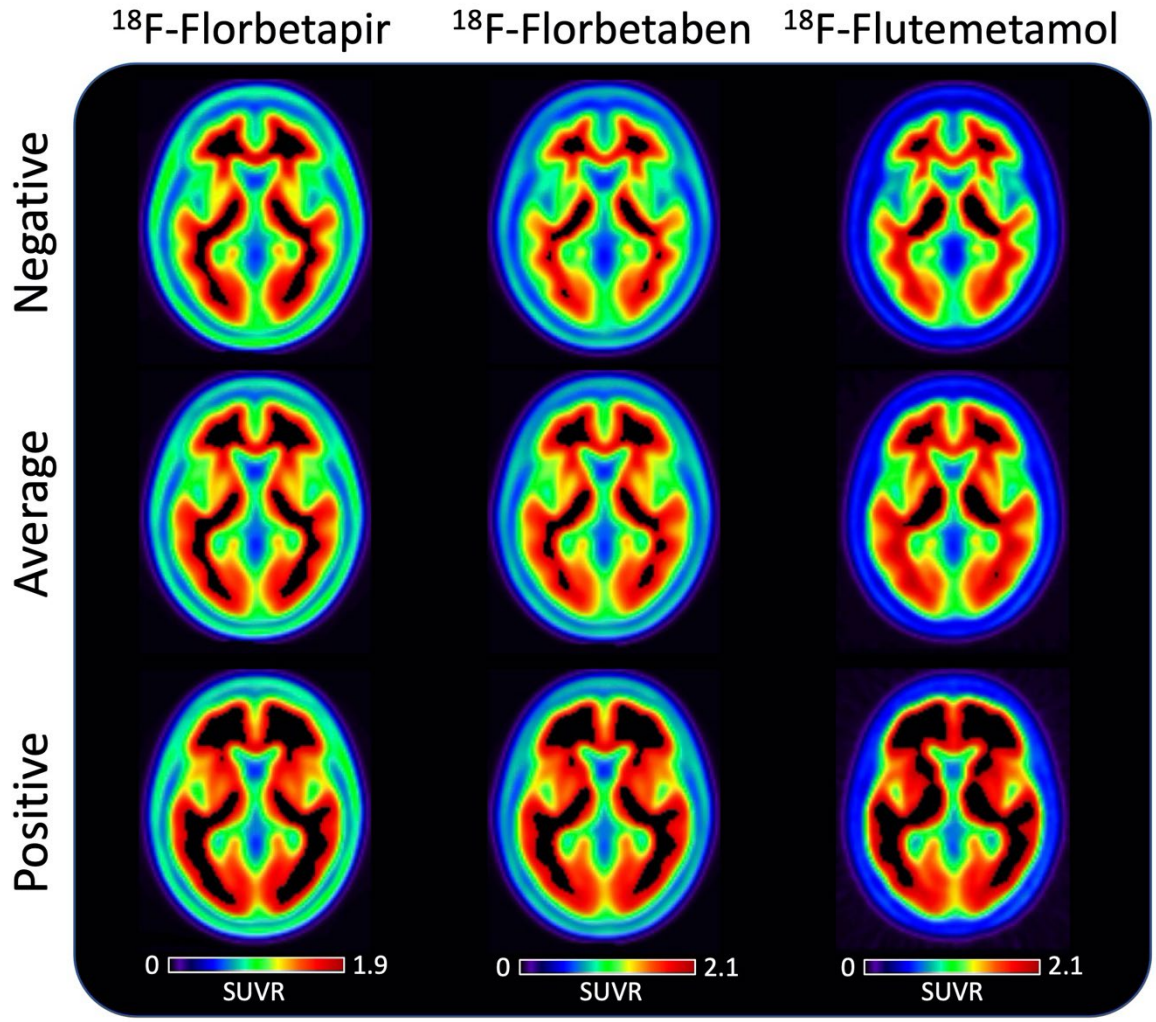

Figure showing a single axial slice for each of the nine templates used in rPOP for the non-linear warping. The grid includes three templates per radiotracer, representing different degrees of amyloid-PET positivity (negative/average/positive). See text for details. Templates are accessible and downloadable at https://github.com/leoiacca/rPOP and at https://neurovault.org/collections/CPHVNXDQ/

Supplementary Figure 2. Non-linear warping rPOP fail in the IDEAS-BHR dataset

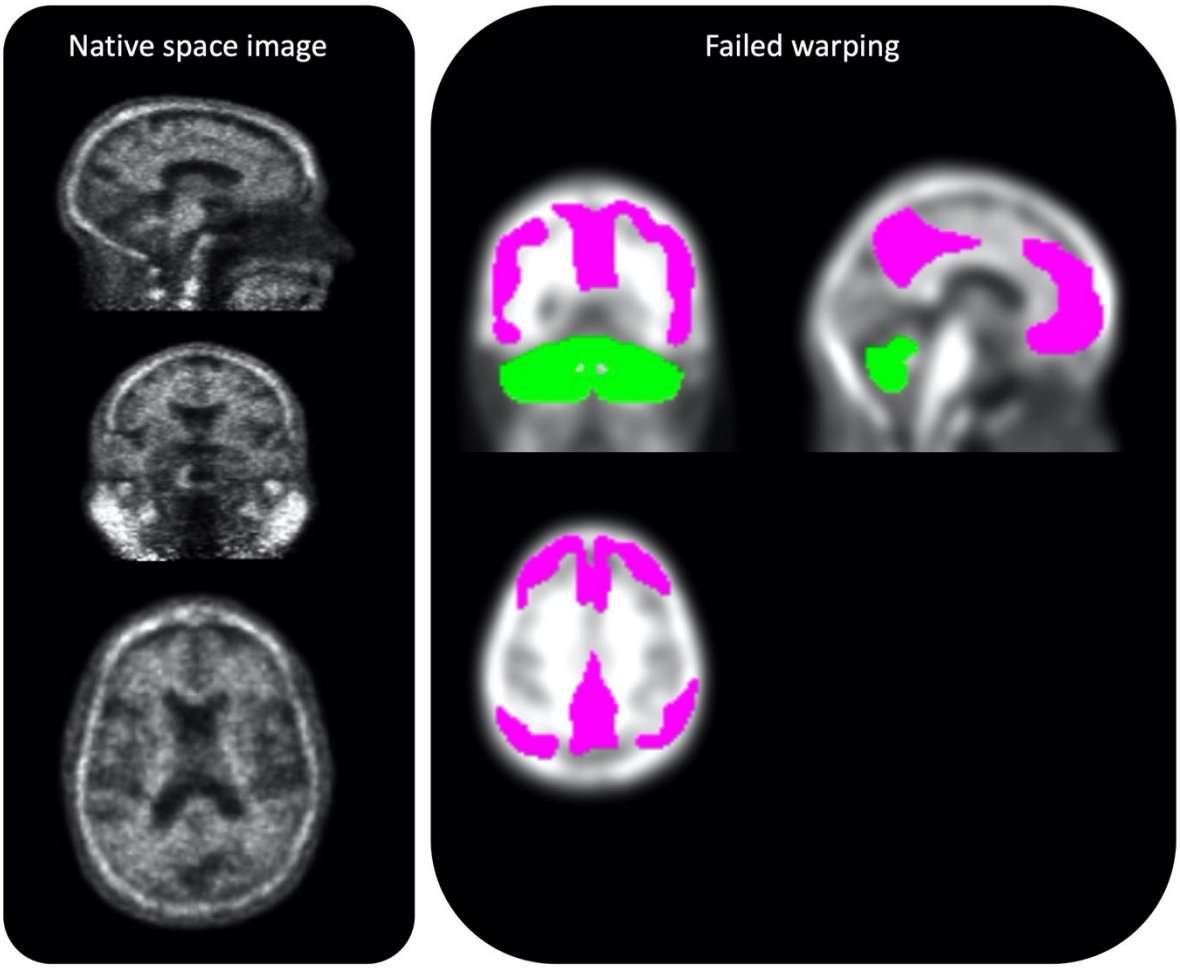

Figure showing the single scan for which rPOP-based non-linear warping failed. Left: Image in its native space as downloaded and converted. Image shows clear abnormal extrabrain uptake. Right: Quality Control of GAAIN VOIs goodness of fit shows the failed warping. The inaccurate fitting is particularly evident for the cortical VOI (purple), largely overlapping with binding outside the brain, indicating inaccurate deformation of the scan.

Supplementary Figure 3. Examples of rPOP warpings in atypical IDEAS-BHR scans

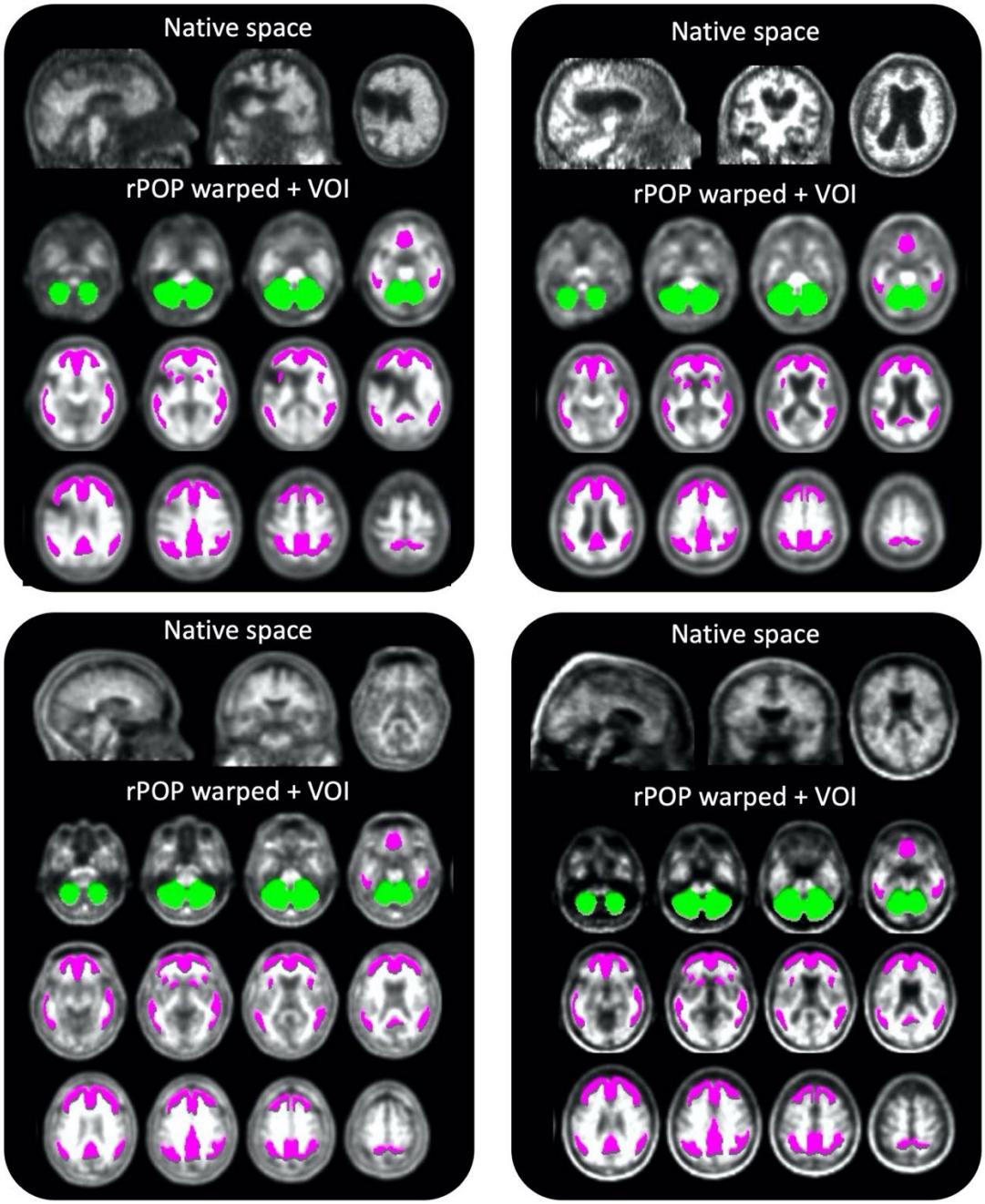

Figure showing accurate non-linear warping performed by rPOP in scans with atypical features. For each panel, top row shows native space scan as was entered in rPOP, bottom rows show respective multislice axial view with GAAIN VOI overlay on the rPOP warped and smoothed scan. In all cases, despite the atypical/abnormal image features, rPOP achieved an accurate warping to the standard space. Top left: scan showing focal area without tracer retention in the left hemisphere, likely representing an old stroke. Bottom left: scan showing high and distributed binding outside the brain. Top right: scan showing significant atrophy with profound ventricular enlargement. Bottom right: scan showing a posterior>anterior binding gradient in the skull, likely due to an error in attenuation correction.

Supplementary Figure 4. Examples of automated differential smoothing

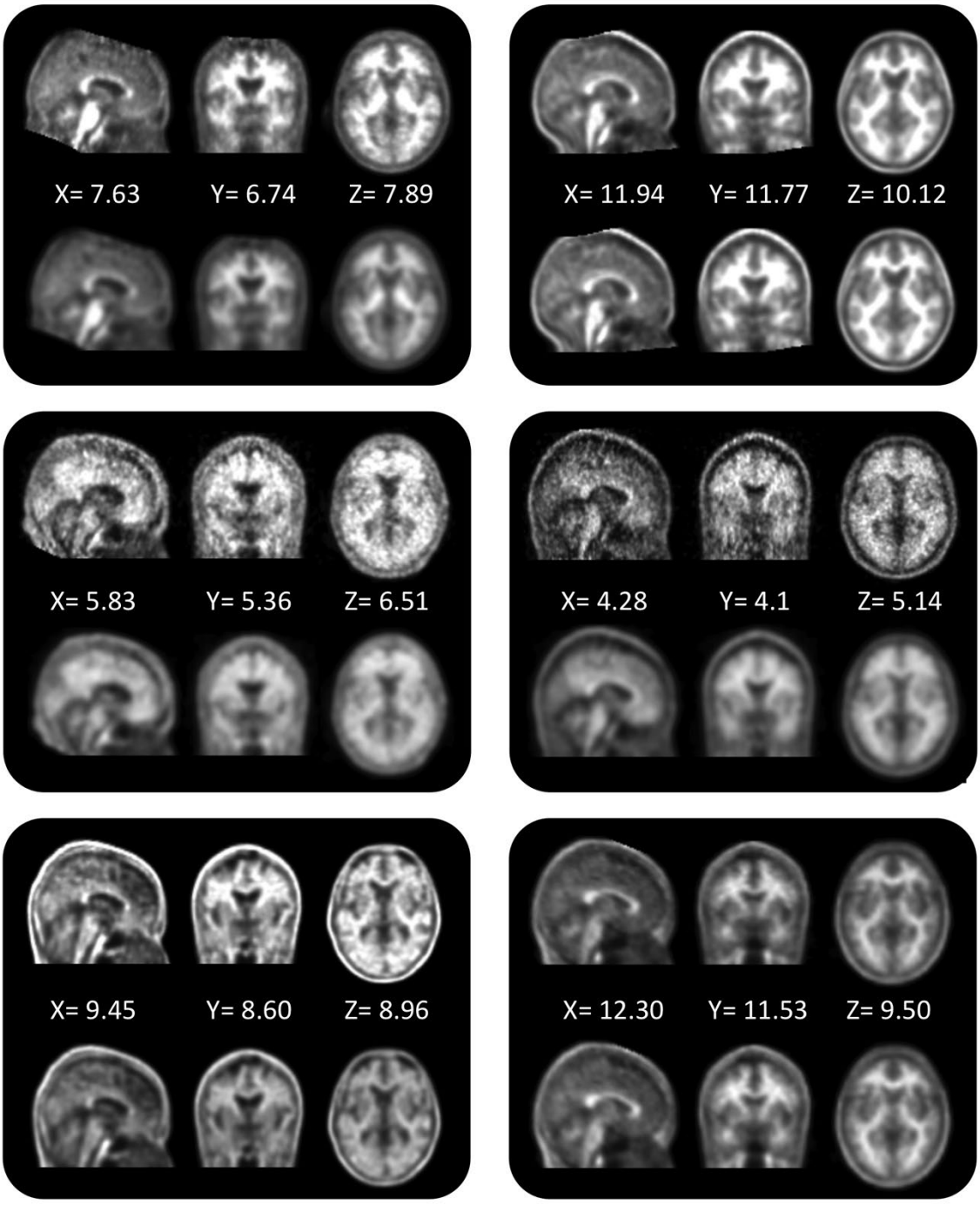

Figure showing six examples of 3dFWHMx-based FWHM estimation and respective smoothed images. For each panel, top row is the (warped) image in the native resolution, center values show estimated FWHM for each plane and bottom row is the corresponding differentially smoothed image using ~10mm^3 as target. No additional smoothing was applied in case the estimation of the native FWHM was already >10. See text for details.

Supplementary Figure 5. Example of stretching artifact in the cerebellum

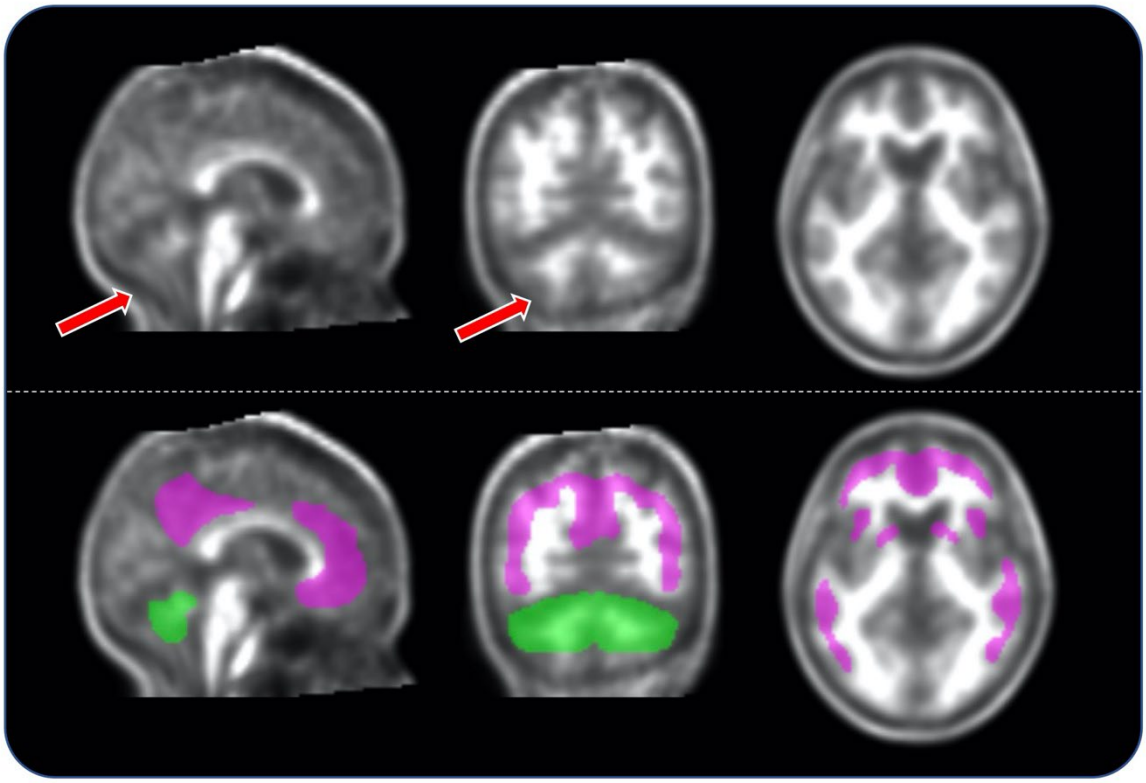

Figure showing a representative example of a stretching artifact in the cerebellum/brainstem observed in a warped image. Top row highlights the artifact (red arrows), particularly visible on the sagittal plane. Bottom row shows an appropriate fit of the GAAIN VOIs despite the artifact.

Supplementary Figure 6. Cross-validation of overall concordance and Cohen's k according to adopted Centiloids thresholds

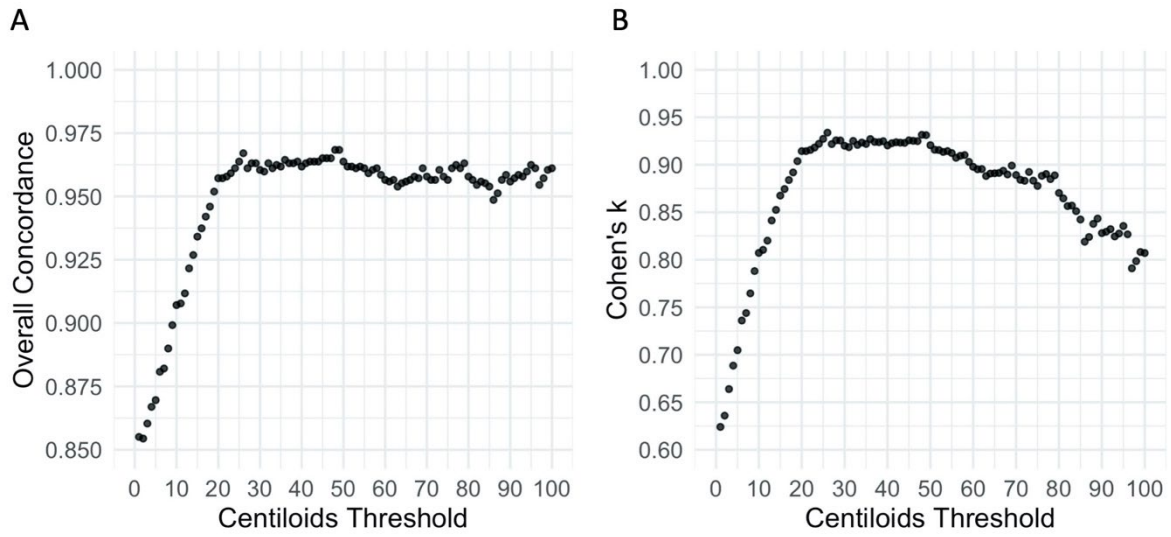

Figure showing a cross-validation of overall concordance and Cohen's k between amyloid status defined according to different thresholds using ADNI PETCore vs. rPOP-based Centiloids.

Supplementary Figure 7. Interaction between native FWHM estimation and rPOP-based Centiloids in predicting ADNI MRI-based Centiloids

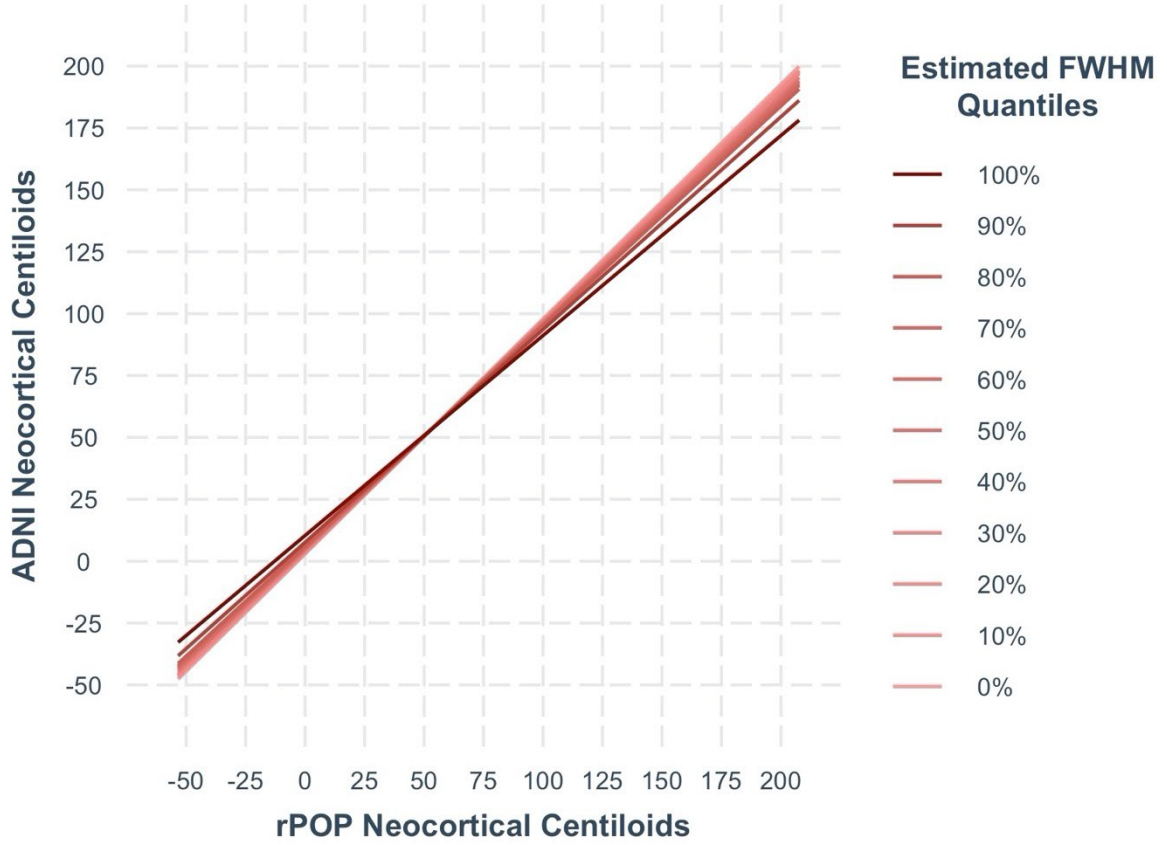

Figure showing association between rPOP-based and MRI-based Centiloids in ADNI according to quantile of estimated FWHM (100%: lowest resolution, 0% highest resolution). The interaction shows that in scans with higher resolution the association between rPOP vs. MRI-based Centiloids is closer to identity.

Supplementary Figure 8. Additional examples of spatial correlation between rPOP- and MRI-based amyloid-PET warped scans

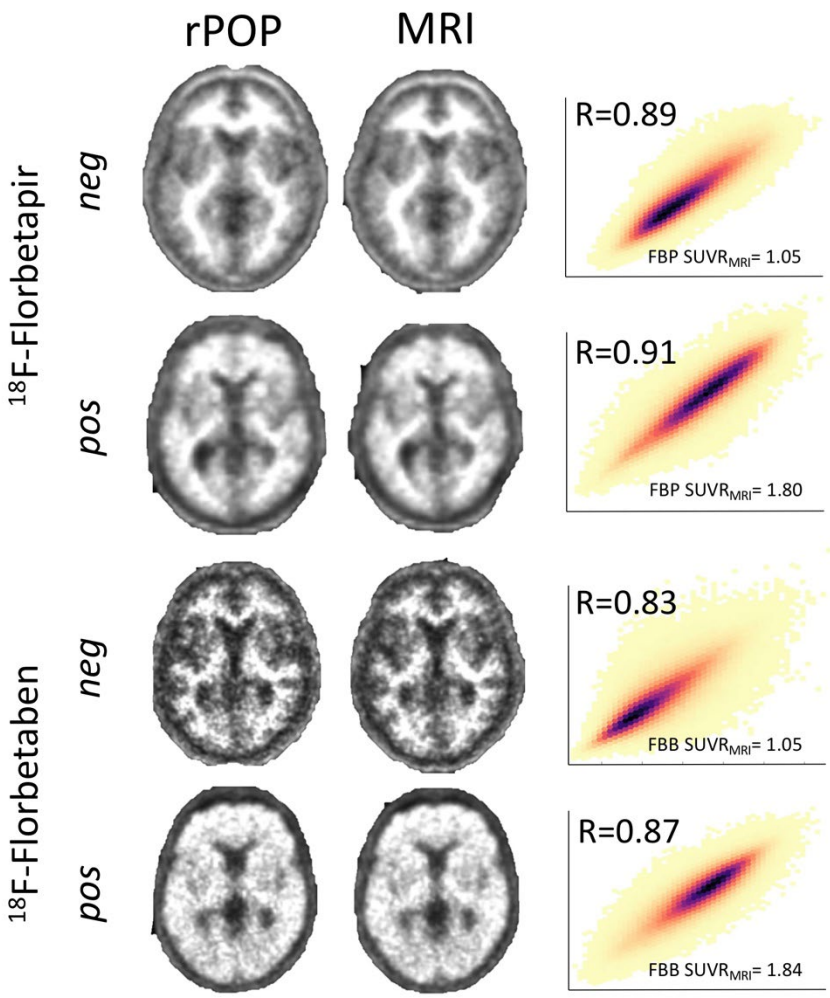

Figure shows four ADNI amyloid-PET scans warped either via rPOP-based or via the standard MRI-based approach, with the respective voxelwise linear correlation and hexed scatterplot. These scans were selected as one random positive and one random negative scan per tracer. See text for details.

Supplementary References

Battle, M.R., Pillay, L.C., Lowe, V.J., Knopman, D., Kemp, B., Rowe, C.C., Doré, V., Villemagne, V.L., Buckley, C.J., 2018. Centiloid scaling for quantification of brain amyloid with [18F]flutemetamol using multiple processing methods. EJNMMI Research 8, 107. https://doi.org/10.1186/s13550-018-0456-7

Klunk, W.E., Koeppe, R.A., Price, J.C., Benzinger, T.L., Devous, M.D., Jagust, W.J., Johnson, K.A., Mathis, C.A., Minhas, D., Pontecorvo, M.J., Rowe, C.C., Skovronsky, D.M., Mintun, M.A., 2015. The Centiloid Project: Standardizing quantitative amyloid plaque estimation by PET. Alzheimer's & Dementia 11, 1-15.e4. https://doi.org/10.1016/j.jalz.2014.07.003

Navitsky, M., Joshi, A.D., Kennedy, I., Klunk, W.E., Rowe, C.C., Wong, D.F., Pontecorvo, M.J., Mintun, M.A., Devous, M.D., 2018. Standardization of amyloid quantitation with florbetapir standardized uptake value ratios to the Centiloid scale. Alzheimers Dement 14, 1565–1571. https://doi.org/10.1016/j.jalz.2018.06.1353

Roalf, D.R., Moberg, P.J., Xie, S.X., Wolk, D.A., Moelter, S.T., Arnold, S.E., 2013. Comparative accuracies of two common screening instruments for the classification of Alzheimer's disease, mild cognitive impairment and healthy aging. Alzheimers Dement 9, 529–537. https://doi.org/10.1016/j.jalz.2012.10.001

Rowe, C.C., Doré, V., Jones, G., Baxendale, D., Mulligan, R.S., Bullich, S., Stephens, A.W., De Santi, S., Masters, C.L., Dinkelborg, L., Villemagne, V.L., 2017. 18F-Florbetaben PET beta-amyloid binding expressed in Centiloids. Eur J Nucl Med Mol Imaging 44, 2053–2059. https://doi.org/10.1007/s00259-017-3749-6